Friction

Research Article

On the multi-scale nature of ski–snow friction in cold conditions

Kalle Kalliorinne[1], Gustav Hindér[1], Joakim Sandberg[1], Hans-Christer Holmberg[2], Roland Larsson[1], Andreas Almqvist[1,3,✉]

Cite this article: Kalliorinne K, Hindér G, Sandberg J, et al. *Friction* 2025, **13**(9): 9441069. https://doi.org/10.26599/FRICT.2025.9441069

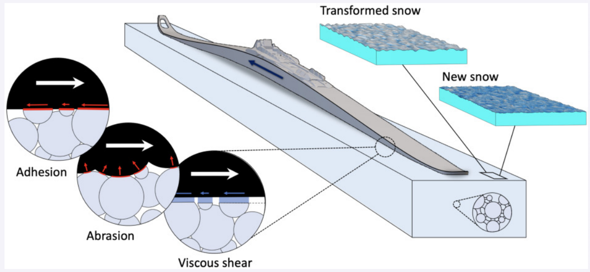

ABSTRACT: In the Olympic winter sports cross-country skiing and the biathlon, athletes aim to minimise resistive forces such as aerodynamic drag, gravity, and ski–snow friction to enhance performance. Ski–snow friction is complex, involving multiple friction mechanisms that vary depending on snow conditions. In cold environments, where the moisture and water content are minimal, friction is presumably influenced primarily by dry interactions between the ski and snow, particularly through adhesion and abrasion at the micro-scale. Here, we examined ski–snow friction under cold conditions using eight pairs of cross-country skis, with different apparent contact lengths and real contact areas. Our findings revealed that apparent contact length, a macro-scale parameter, had the greatest impact on friction, followed by total real contact area, which is a multi-scale parameter. For snow temperatures below approximately −10 °C, longer apparent contact lengths reduced friction, whereas shorter lengths are more effective above −10 °C. In addition, at −3 °C, minimising the total real contact area was advantageous for reducing friction, while this effect diminished at −8.5 °C. At the coldest tested temperature of −13 °C, a larger total real contact area resulted in the lowest friction. These findings highlight the importance of considering both macro- and micro-scale contact properties for optimising ski performance in different cold conditions.

KEYWORDS: winter sports; cross-country ski; snow; adhesive; abrasive; friction; RTK-GNSS

1 Introduction

In most winter endurance sports, the goal is to move from point A to B in the shortest time possible. To complete the distance, the athletes must overcome resistive forces acting on them. These usually include aerodynamic drag and the gravitational force in inclined parts of the track. Friction is typically a third resistive force, arising in the sliding contact between the equipment and the snow or ice counter-surface [1]. At the highest level of cross-country skiing, where time differences can be small, even a slight reduction in resistive forces can significantly impact the race result [2].

Ski–snow friction is a complex matter that involves several proposed friction mechanisms, namely adhesive friction, abrasive friction, viscous friction, friction due to compaction, and capillary friction [1]. Adhesive friction is caused by shearing the ski base and snow contact interface, often referred to as “dry friction” [3–6]. Abrasive friction is caused by moving or plastically deforming the snow at a smaller scale [7–9]. Viscous friction results from shearing the thin water film between the ski base and the snow surface; this water film may either preexist or be friction-induced by melting. Friction due to compaction is caused by plastic deformation at a larger scale of the snow surface while sliding forward.

To predict the performance in cross-country skiing, the skis need to be quantified in terms of various parameters. Since skis deform significantly under load, a ski-camber profile measurement can be helpful to roughly estimate the size of the contact interface, also known as the apparent contact area [10–14]. For a more precise estimate of the apparent contact area, numerical simulation of the macro-scale contact can be employed [15]. However, their ski-base texture needs to be characterized to determine how the real contact area differs between skis. By using surface measurements of the ski-base texture in numerical contact simulations, several mechanical parameters of micro-scale contact can be quantified, namely real contact area, average interfacial separation, and reciprocal interfacial separation [16–19]. By combining the ski-camber profile and the ski-base texture’s interaction with the snow, i.e., mechanical properties of macro- and micro-scale contacts, a description for the entire system can be obtained, which can be linked to friction mechanisms [20].

There are several ways to measure the friction force between a material sample and snow/ice. However, options for measuring ski–snow friction with full-sized skis are limited. One method

[1] Division of Machine Elements, Luleå University of Technology, Luleå 97187, Sweden. [2] Division of Health, Medicine and Rehabilitation, Luleå University of Technology, Luleå 97187, Sweden. [3] Swedish Olympic Committee, Stockholm 11433, Sweden.

✉ Corresponding author. E-mail: andreas.almqvist@ltu.se

Received: September 21, 2024; Revised: December 28, 2024; Accepted: January 22, 2025

Nomenclature

A_r	Real contact area	m^2	$\min(\bar{h})$	Minimum average interfacial separation	m
A_{tot}	Total real contact area	m^2	L_a	Apparent contact length	m
A_p	Projected contact area	m^2	n	Porosity	%
A_w	Wetted area	m^2	P	Apparent pressure	Pa
$\overline{A_w/h}$	Average reciprocal interfacial separation	m	$\bar{P}$	Mean apparent pressure	Pa
d_s	Snow grain diameter	m	T_s	Snow temperature	°C
E	Elastic modulus	Pa	V	Velocity	m/s
F_{tot}	Total friction force	N	W	Width of the ski	m
$F_{adhesive}$	Adhesive friction force	N	η	Viscosity	Pa·s
$F_{abrasive}$	Abrasive friction force	N	μ	Coefficient of friction (COF)	—
H	Hardness	Pa	τ	Shear strength	Pa

involves using a linear ski tribometer [21–26], which operates by sliding a single ski over a long bed of snow. This setup offers the consistency of a controlled laboratory test, as it eliminates the variability introduced by changing weather and snow conditions. The drawback with this method is that the sliding distance is relatively limited, and friction is measured under a forced constant velocity. Another technique for quantifying ski–snow friction involves equipping a sled with a pair of skis [27–30], and either measuring or calculating the friction based on some other parameter.

The primary objective of this study was to quantify the ski–snow coefficient of friction (COF) of eight pairs of skis under cold conditions, and adhesive, abrasive, and viscous friction are considered the primary mechanisms. By understanding these relationships, the study aims to provide guidelines for optimizing ski design and performance in varying environmental conditions. To achieve this, the present work utilized the measurement technique developed in Ref. [30] and four mechanical characteristics of ski–snow contact, including apparent contact length and real contact area, determined using the method developed by Kalliorinne et al. [15, 19, 20]. These measurements, conducted under cold conditions with air and snow temperatures below zero, are intended to provide actionable insights into the factors that most significantly affect ski performance.

2 Method

The method section is divided into two parts. The first part covers derivation of contact mechanical parameters used to characterize the multi-scale nature of the skis, and the second details the protocol for field tests, including preparation of skis and track.

2.1 Multi-scale ski characterization

A set of eight pairs of purpose-built test skis from Fischer Sports, model Speedmax 192 Skate, was selected for this study. This selection was made to ensure as consistent dynamic behaviour as possible across all pairs. The skis were all labelled to have the same ski-base material. However, this does not guarantee uniform ski-base quality, which is a challenging parameter to control.

The characterization is divided into three parts. It starts with the marco-scale perspective, encompassing the ski-camber profile and ski mechanics, herein characterized by the apparent contact length, L_a. Then the micro-scale topography is characterized in terms of seven common surface roughness parameters. Finally, the scales are coupled and a multi-scale analysis, presenting three contact mechanical response parameters, including the real contact area, A_{tot}, connected to snow-friction mechanisms, is conducted.

The micro-, macro-, and multi-scale contact mechanical response parameters are computed by means of the boundary element method (BEM)-based approaches developed in Refs. [15, 19, 20]. These enable simulations of detailed ski–snow interactions, providing insights into contact mechanics that are critical for understanding frictional behaviour.

2.1.1 Macro-scale analysis

The ski-camber profiles (of all sixteen skis within the set) were measured using a ski-camber height profilometer (SkiSelector Sportdata AB, Sweden). Numerical simulations of the macro-scale contact between the skis and snow were performed using the BEM developed in Ref. [15]. In this case, the model utilizes the measured ski-camber profile and simulates the ski–snow contact with a smooth and perfectly flat snow-counter surface. The simulations were carried out assuming a ski-base stiffness of $E_{base} = 900$ MPa, a relatively stiff snow-counter surface of $E_{snow} = 200$ MPa [31], and a Poisson ratio of $\nu = 0.3$ for both surfaces.

Figure 1 depicts the macro-scale ski-camber profiles (H) and the simulated pressure distributions (P)—termed the apparent pressure, since the simulation only considers the ski-camber profile (macro-scale) and not the topography of the ski-base structure (micro-scale), for three of the skis, i.e., Ski 3A, Ski 6A, and Ski 8A. Both H and P are functions of the coordinate X along the whole length Ω of ski. See Appendix for all skis, and Table 1 for a list for the average of each ski pair's apparent contact length.

2.1.2 Micro-scale analysis

Each ski in the selected set of ski pairs was stone ground using a Tazzari Albatros RP 23 ski-grinding machine. The grinding protocol was configured to produce three different textures, denoted Grind 1 (G1), Grind 2 (G2) and Grind 3 (G3), see Table 1. Note that the ski pairs with the same grinding settings were ground after each other on the same stone to make the grinds as consistent as possible.

The grinds were specified to generate textures with significantly different load-bearing area, i.e., surface height probability distributions of different breaths (for concrete illustrations, see, e.g., Refs. [24, 32]), with the intention that G1 should have the broadest and G3 the narrowest. The corresponding micro-scale ski-base textures $h = h(x, y)$, where (x, y) are the micro-scale coordinates belonging to the domain ω, are illustrated in Fig. 2. These are obtained with a Zygo NewView 9000 white light interferometer (WLI), where a single-shot measurement corresponds to the area $A_t = |\omega| = 6.3\ \text{mm} \times 6.3$ mm, with a resolution of $1{,}000 \times 1{,}000$ pixels.

Table 2 presents seven commonly used surface roughness parameters for each pair of skis (pair 1–8) and grind (G1, G2, and G3). The values are the mean values of the surface roughness parameters calculated for 10 surface roughness measurements (5 from each ski) of each pair obtained using the same method as in Ref. [19]. It is clear that the parameter values are not consistent for the different grinds as they are produced and measured at different locations on different skis.

The average of the mean surface roughness parameters for each of the grindings (presented in Table 2) is presented in Table 3.

An analysis of the average of the mean surface roughness parameters reveals the following.

(1) Grind G1 exhibits the highest mean average roughness value (S_a) of 5.5 μm, and positive skewness (S_{sk}) of 0.5. The kurtosis (S_{ku}) of G1 is 2.2, which is narrower than that of normal ($S_{ku} = 3$) distribution of peak heights. G1 also has the highest root mean square gradient (S_{dq}) of 139 μm/mm, indicating steeper surface grooves. Grind G1 possesses the highest reduced peak height (S_{pk}) of 9.5 μm and the lowest reduced valley depth (S_{vk}) is 2.4 μm, which is in alignment with the skewness value, indicating a surface with more peaks than valleys. The core roughness depth (S_k) of 12.3 μm and the sum of three core-roughness parameters being the largest correlate with the highest S_a value.

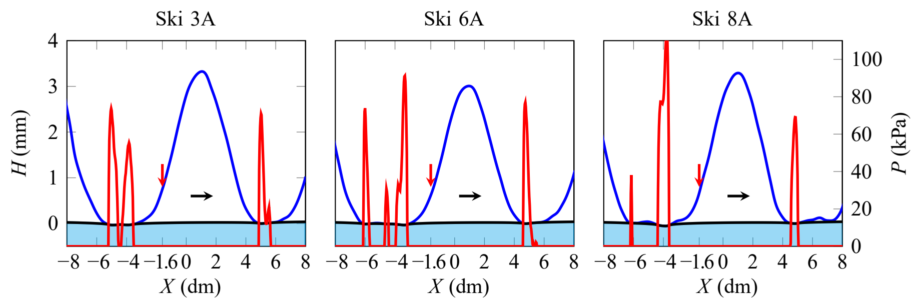

Fig. 1 Macro-scale contact response in terms of ski-camber profiles (H) and corresponding pressure distributions (P) of three different skis under an equivalent load of 40 kg, located 1.6 dm behind the balance point. The snow-counter surface is modelled using an elastic modulus of $E_{snow} = 200$ MPa. The determined apparent contact lengths of Ski 3A, Ski 6A, and Ski 8A are 227, 235, and 140 mm, respectively.

Table 1 Average apparent contact length for each ski pair

Ski pair	Grind	L_a (mm)
1	G1	232
2	G2	198
3	G3	221
4	G1	260
5	G2	266
6	G3	226
7	G1	147
8	G3	135

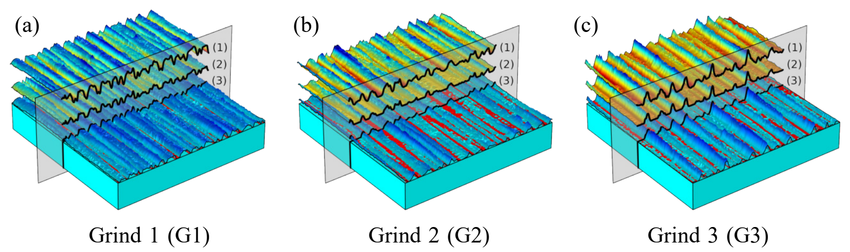

Fig. 2 Illustration of typical surface topographies ($h(x,y)$) corresponding to three ski-base grinding patterns ((a) G1, (b) G2, and (c) G3), shown in three analytical layers: (1) ski-base texture, with a colour map showing valleys (recesses) in blue and ridges (protrusions) in red; (2) texture pressed against smooth ice (not visible); (3) texture pressed against smooth ice, but with contact points coloured red and shades of blue showing the height of gap between surfaces. The colour maps for each grind are set individually to best highlight features, but the height scale is consistent across all three, enabling direct comparison of cross-sectional profiles.

Table 2 Mean values of surface roughness parameters calculated from 10 surface roughness measurements

Ski pair	Grind	S_a (μm)	S_{sk}	S_{ku}	S_{dq} (μm/mm)	S_{pk} (μm)	S_k (μm)	S_{vk} (μm)
1	G1	5.4	0.6	2.3	146.4	10.3	11.7	2.2
2	G2	4.9	0.1	2.2	117.3	4.5	15.3	3.1
3	G3	4.8	−1.1	3.5	115.9	2.2	10.0	11.8
4	G1	5.6	0.6	2.2	147.0	10.2	12.1	2.4
5	G2	5.3	0.3	2.1	138.4	5.6	15.5	3.0
6	G3	4.7	−0.9	3.2	115.9	2.6	11.7	10.0
7	G1	5.4	0.4	2.1	123.0	8.0	13.1	2.7
8	G3	4.3	−1.0	3.4	99.0	2.3	9.8	9.9

https://doi.org/10.26599/FRICT.2025.9441069 Tsinghua University Press | SciOpen

(2) Grind G2 has an S_a-value of 5.1 μm, which is slightly lower than G1's, yet larger than G3's. An S_{sk}-value of 0.2, reflecting a balanced distribution of peaks and valleys. The kurtosis (S_{ku}) of G2 equals the one of G1, but its root mean square gradient (S_{dq}) of G2 is 128 μm/mm, being lower. Grind G2 has a smaller difference between the S_{vk} and S_{pk}-values than G1, but it exhibits the highest core roughness depth ($S_k = 15$ μm).

(3) Grind G3 shows the lowest average roughness value (S_a) of 4.6 μm and a negative skewness (S_{sk}) of −1.0, indicating a surface with more valleys than peaks. The kurtosis (S_{ku}) for G3 is 3.4, the highest among the grinds. The root mean square gradient (S_{dq}) for G3 is 110 μm/mm, the lowest among the grinds, and the reduced peak height (S_{pk}) is 2.4 μm. G3 also has the lowest core roughness depth (S_k) of 10.5 μm but the highest reduced valley depth (S_{vk}) of 10.6 μm, indicating significant valley depths.

The contact mechanical response for the 30 measurements of the ski-base textures was simulated using the BEM-based method described in Ref. [19]. The simulations were conducted with a ski-base stiffness of $E_{base} = 900$ MPa, an ice-counter surface stiffness of $E_{ice} = 9$ GPa, and a Poisson ratio of $\nu = 0.3$ for both surfaces. While testing, the track exhibited an icy mirror-like surface and a porosity of $n = 0\%$ was used when post-processing the data.

Three micro-scale contact mechanical response parameters, considered functions of the apparent contact pressure (based on all of the 10 measurements), were selected. These are fractional real contact area $\mathcal{A}_n = A_{r,n}/A_t$, where $A_t = 6.3$ mm × 6.3 mm, average interfacial separation $\bar{h}_n$, and average reciprocal interfacial separation $\overline{1/h_n}$. Figure 3 depicts these for three individual skis (Ski 1B, Ski 2B, and Ski 3B) with ski-base textures G1, G2, and G3, respectively.

Although the micro-scale contact mechanical response parameters do not discriminate the grinds statistically, the surface roughness parameters (Table 3) confirm that the grinding protocols successfully created distinct surface textures likely to exhibit different frictional behaviours.

2.1.3 Multi-scale analysis

Utilizing the multi-scale analysis developed in Ref. [20], the total real contact area $A_{tot,n}$, minimum average interfacial separation $\min(\bar{h}_n)$, and integrated average reciprocal interfacial separation $\overline{A_w/h}$ were calculated for zero snow porosity, i.e., $n = 0\%$. This method is based on evaluating parameters h_n, $A_{r,n}$, and wetted area A_w, approximated using $A_{r,n}$, as functions of position ($X \in \Omega$) all along the ski-camber geometry. Then these are obtained by integration. More precisely, $A_{tot,n}$ is obtained by integrating the fractional real contact area ($\mathcal{A}_n$), with respect to X, i.e.,

$$A_{tot,n} = L_w \int_{\Omega} \mathcal{A}_n(X)\,dX \tag{1}$$

where L_w is the width of the ski. The minimum of the average interfacial separation, $\bar{h}_n(X)$, which is as a function of X, is obtained via Eq. (2):

$$\min(\bar{h}_n(X)) = \frac{1}{A_t}\int_{\omega} h_n(x,y)\,dxdy + \min(H(X)) \tag{2}$$

where ω is the micro-scale domain with area $A_t = 6.3$ mm × 6.3 mm). Similarly, the average reciprocal interfacial separation $\overline{A_w/h_n}$ is given by

$$\overline{A_w/h_n} = L_w \int_{\Omega}\left(\frac{1-n}{A_g}\int_{\omega_g}\frac{dxdy}{h_n(x,y)+H(X)}\right)dX \tag{3}$$

where A_g is the area of the micro-scale domain with a gap between the surfaces (and possibly solid–liquid contact).

It should be noted that it is irrelevant to equate the averaged mean values and standard deviations for the multi-scale parameters listed in Table 4, as their variability is inherited from both macro- and micro-scale properties.

2.2 Field testing

The main stages of the measurement procedure with the free-gliding sled-based method are described in the subsections below. Some photos taken during the measurement campaign are depicted in Fig. 4.

2.2.1 Ski preparation

Preparation of the skis was conducted before each testing session, this step involves a standardized process. First, the skis are cleaned using a wax remover (SkiGo). Next, a universal liquid glide wax (RedCreek) is applied, followed by brushing the skis with a rotor steel brush (RedCreek) and then a rotor nylon brush (RedCreek).

Table 3 Averaged mean values and standard deviations of surface roughness parameters for different grinds (G1, G2, and G3)

Grind	S_a (μm)	S_{sk}	S_{ku}	S_{dq} (μm/mm)	S_{pk} (μm)	S_k (μm)	S_{vk} (μm)
G1	5.5 ± 0.1	0.5 ± 0.1	2.2 ± 0.1	139 ± 11	9.5 ± 1.1	12.3 ± 0.2	2.4 ± 0.2
G2	5.1 ± 0.3	0.2 ± 0.1	2.2 ± 0.1	128 ± 11	5.1 ± 0.6	15.4 ± 0.1	3.1 ± 0.1
G3	4.6 ± 0.2	−1.0 ± 0.1	3.4 ± 0.1	110 ± 9	2.4 ± 0.2	10.5 ± 0.8	10.6 ± 0.8

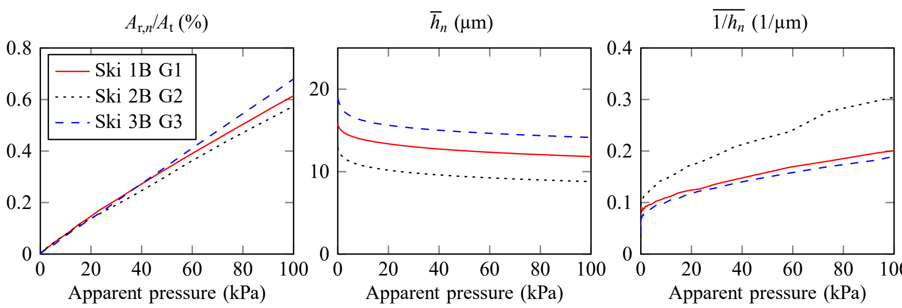

Fig. 3 Three selected contact mechanical response parameters, i.e., fractional real contact area $A_{r,n}/A_t$, average interfacial separation $\bar{h}_n$, and average reciprocal interfacial separation $\overline{1/h_n}$ as a function of apparent contact pressure, all simulated at a porosity of $n = 0\%$. Solid red, dotted black, and dashed blue lines correspond to Ski 1B with grind G1, Ski 2B with grind G2, and Ski 3B with grind G3, respectively.

2.2.2 Track preparation

The sled requires some directional guidance, so the tests are conducted in the classical ski tracks. The track was prepared at least 2 h before testing using a standard cross-country snow groomer. This avoids concurrent sintering and degradation/compaction of the track during testing, which might otherwise influence the measurements.

2.2.3 Ski–snow friction testing

The method developed in Ref. [30], involving releasing the sled from the top of a hill and letting it glide freely until it stops or reaches the end of the track, is adopted here. This method utilizes an RTK-GNSS system to record the sled's position with 1 cm accuracy at a sampling frequency of 5 Hz. The measurement data were used when calculating the COF (according to the procedure outlined in Ref. [30]).

The sled, loaded with 80 kg of Olympic weights, has its centre of mass placed 160 mm behind the balance point, resembling a 80 kg skier in a neutral tucking position [14]. Each pair of skis was tested four times consecutively, and the COF was calculated as the mean of these four measurements.

2.2.4 Environmental conditions

The three test campaigns were conducted in the morning between 8:00 am and 10:00 am on January 30, February 2, and February 9, 2024 ensuring stable snow conditions as the sun remained low in the sky in the northern hemisphere during these months. There was no precipitation during any of the test campaigns, and the snow grain size was measured at the beginning and end of each session, consistently found to be approximately 0.2 mm on all three occasions.

The snow and air temperatures and air humidity were regularly monitored, confirming that the conditions remained stable. On average, the snow temperatures during the three test campaigns were −3, −8.5, and −13 °C; the air temperatures were 1.5, −6, and −15 °C; the air humidity levels were 80%, 70%, and 75%, respectively.

Although no measurement device for wind speed was used, we did not perceive any noticeable wind during the test campaigns and wind speed was deemed negligible.

Table 4 Calculated macro- and multi-scale parameters corresponding to an average ski in the pair

Ski pair	Grind	L_a (mm)	A_{tot} (mm²)	$\min(\bar{h})$ (μm)	$\overline{A_W/h}$ (km)
1	G1	232	26.6	15.2	1.7
2	G2	198	24.0	12.7	1.7
3	G3	221	26.9	9.7	2.4
4	G1	260	23.2	15.3	1.9
5	G2	266	24.7	14.1	2.2
6	G3	226	24.0	10.9	2.1
7	G1	147	24.8	13.8	1.6
8	G3	135	23.2	9.5	1.8

3 Results

In this section, we present and analyse the results from the glide tests conducted during the three measurement campaigns. The results are divided into two parts, with the first presenting analysis of the ski–snow COF estimations, and the second the resulting linear regression model for friction prediction.

3.1 COF estimation

The averaged COF estimated based on the measurements (track height profile, and the position and velocity of the sled) acquired during the glide tests are presented in Table 5, and the subscript on μ (denoting the COF) declares the corresponding snow temperature.

The COF is also illustrated in Fig. 5, and it is plotted against the macro- and multi-scale parameters listed in Table 4. The red, blue, and cyan colours represent measurements taken during the campaigns with snow temperature $T_s = -3$, −8.5, and −13 °C, respectively.

3.2 A COF prediction formula

In this section, we present the results of fitting a linear two-parameter regression model to the COF (μ) using the apparent contact length (L_a) and the total real area of contact (A_{tot}) as predictors. The model was applied to data from three measurement campaigns and the reason for selecting L_a and A_{tot} as predictors will be discussed in the following section. The regression model is expressed as Eq. (4):

$$\mu = C_0 + C_1\tilde{L}_a + C_2\tilde{A}_{tot} \tag{4}$$

where $\tilde{L}_a = (L_a - L_{a\min})/(L_{a\max} - L_{a\min})$ and $\tilde{A}_{tot} = (A_{tot} - A_{tot\min})/(A_{tot\max} - A_{tot\min})$ are normalized representations of L_a and A_{tot}, respectively, and C_0, C_1, and C_2 are coefficients determined through the fitting process.

The constants (C_0, C_1, and C_2) for the fitted models under the three different snow temperatures are presented in Table 6. It is evident that the model behaves differently on the three occasions.

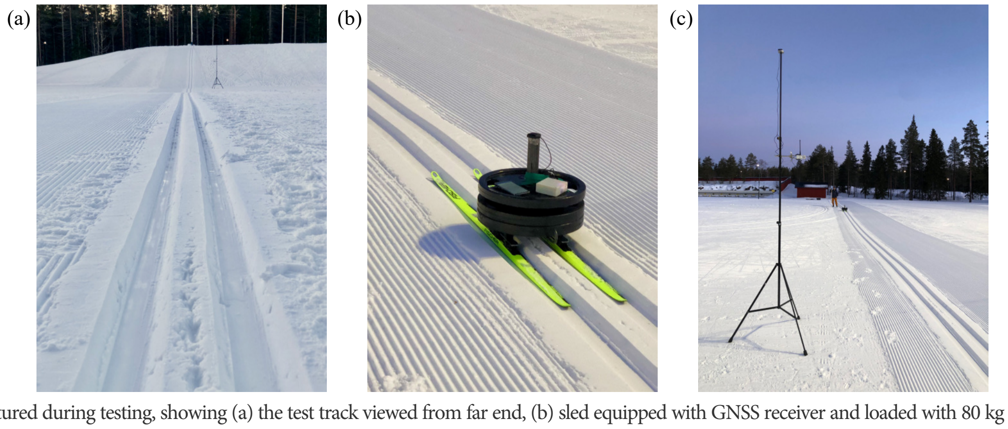

Fig. 4 Pictures captured during testing, showing (a) the test track viewed from far end, (b) sled equipped with GNSS receiver and loaded with 80 kg of weights, with its centre of mass placed 160 mm behind balance point, and (c) base station with GNSS receiver located in the middle of track, less than 35 m away from all surveyed positions, ensuring optimal radio transmission and highest accuracy of RTK corrections.

Specifically, the constant C_0 increases with decreasing temperature; constants C_1 and C_2 are positive at $T_s = -3$ °C and $T_s = -8.5$ °C, but negative at $T_s = -13$ °C; C_2 at $T_s = -8.5$ °C has the smallest absolute value.

Table 5 Resulting coefficient of friction (multiplied by 10^2) at each test campaign: μ_{-3}, $\mu_{-8.5}$, and μ_{-13}, for all eight ski pairs, with pair 5 identified as an outlier

Ski pair	Grind	μ_{-3} (10^{-2})	$\mu_{-8.5}$ (10^{-2})	μ_{-13} (10^{-2})
Pair 1	G1	3.42	3.62	4.35
Pair 2	G2	3.26	3.37	4.46
Pair 3	G3	3.36	3.40	4.28
Pair 4	G1	3.45	3.55	4.36
Pair 5	**G2**	**3.05**	**3.29**	**4.44**
Pair 6	G3	3.18	3.34	4.44
Pair 7	G1	3.12	3.08	4.49
Pair 8	G3	2.86	3.14	4.57

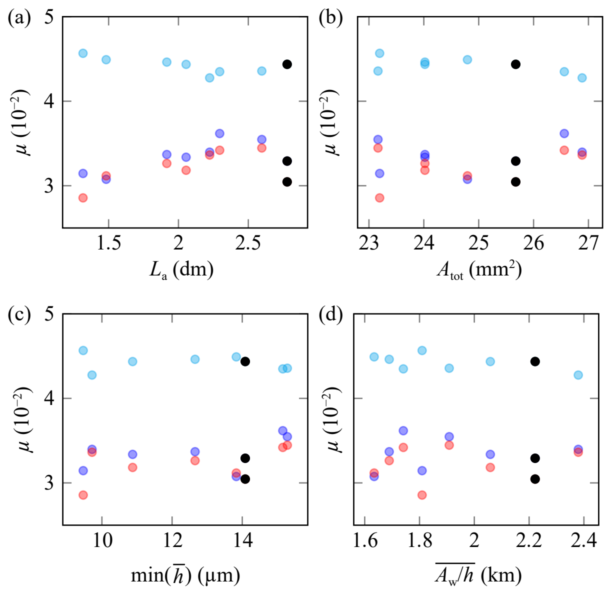

Fig. 5 (a) Coefficient of friction versus apparent contact length L_a, (b) real contact area A_{tot}, (c) minimum average interfacial separation $\min(\bar{h})$, and (d) integrated average reciprocal interfacial separation $\overline{A_w/h}$. Red marks represent measurements taken at $T_s = -3$ °C, blue marks measurements taken at $T_s = -8.5$ °C, and cyan marks measurements taken at $T_s = -13$ °C. The black mark denotes data points that were removed from the dataset.

Figure 6 displays the model's performance through a regression plot. A well-fitting model would have all points aligned with the black line, while a significant spread or deviation suggests model limitations. The results indicate the best performance at $T_s = -13$ °C, with a relative root mean square error of 0.48%, while the largest error occurs at $T_s = -8.5$ °C, reaching 2.15%.

Figure 7 shows a surface map of COF using the model in Eq. (4) and three sets of constants are presented in Table 6. The dots on the surface represent the L_a and A_{tot} data of each ski pair (Table 4), roughly indicating the model's usability. A dark blue colour on the surface map represents the lowest coefficient of friction, ranging to the highest values represented by a yellow colour. Note that the colour maps are individually set for each snow condition. The level curves are set with 0.1×10^{-2} increments.

4 Discussion

In the following, we first discuss the estimation of the COF, then the fitted models for each of the measurement campaigns, and the model's performance across different snow conditions. Thereafter, a general discussion follows.

4.1 On the COF estimation results

Here we examine the patterns observed in the COF on the three occasions, with snow temperatures −3, −8.5, and −13 °C, with respect to the macro- and multi-scale contact mechanical parameters listed in Table 4. The apparent contact length (L_a) and total real contact area (A_{tot}) are given particular focus.

Considering each measurement campaign separately, the data presented in Fig. 5, except for pair 5, suggest a linear relationship between COF and apparent contact length. The reason that pair 5, which is illustrated with black dots, diverges from this pattern,

Table 6 Constants C_0, C_1, and C_2, obtained from fitting the model in Eq. (4) under different snow conditions

T_s (°C)	$C_0 (10^{-2})$	C_1	C_2
−3	2.925	0.578	0.117
−8.5	3.083	0.562	0.040
−13	4.572	−0.231	−0.115

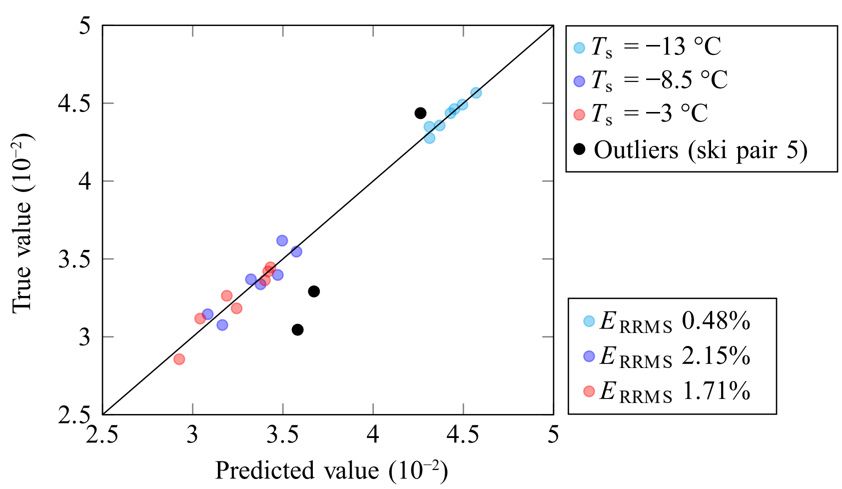

Fig. 6 Illustration of model accuracy: a perfect model aligns data on the black line with random error scattering data around the black line and systematic errors showing a clear divergence from the black line. The performance of models is evaluated in terms of relative root mean square (RRMS) error (E_{RRMS}).

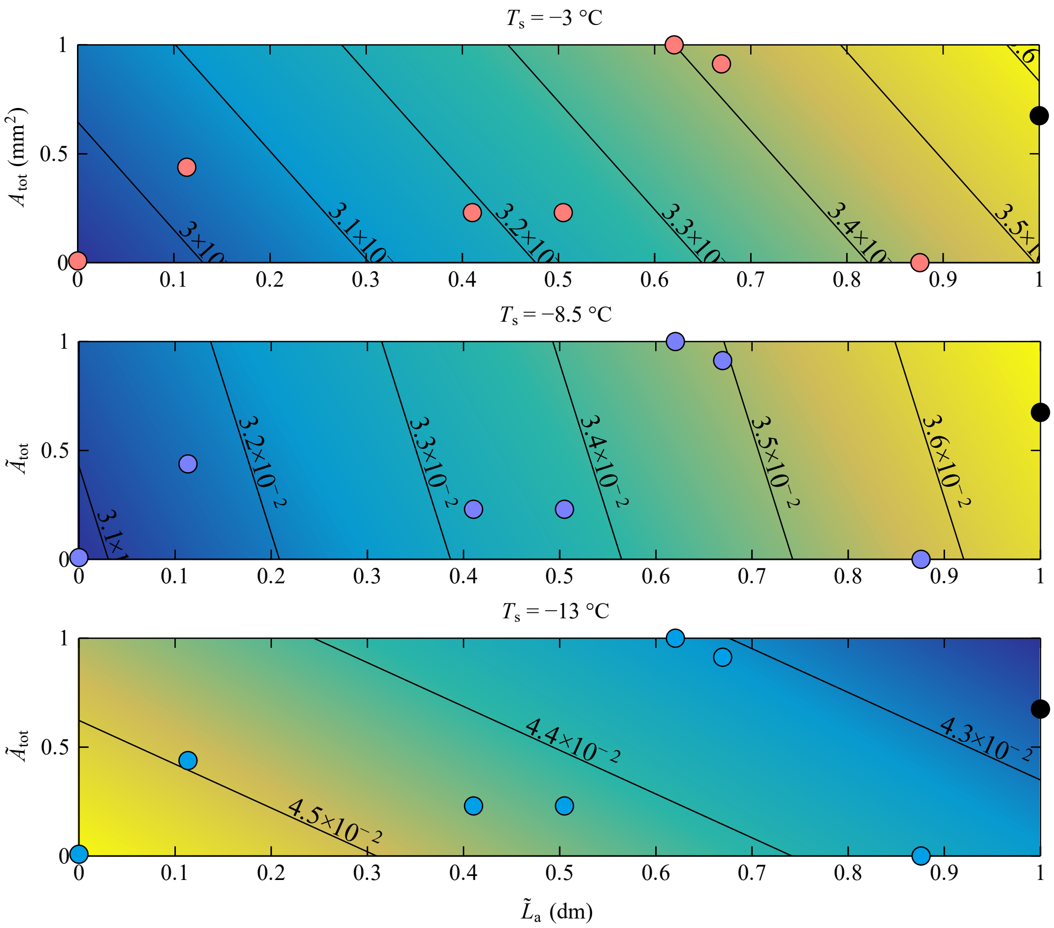

Fig. 7 Topology map of coefficient of friction μ as a function of normalised apparent contact length $\tilde{L}_a$ andnormalised total real contact area $\tilde{A}_{tot}$ for one ski under half load, i.e., 40 kg, at 3 different snow temperature T_s conditions.

could either be because it is an outlier or there is an optimum around $L_a = 2.5$ dm, but it would not be wise to draw conclusions based on one data point.

For the other contact mechanical response parameters plotted in Fig. 5, it is difficult to identify patterns. This could be because, as it seems from the data, the apparent contact length has the most significant influence on the COF and thus the influence of the other parameters drawn in the variation of L_a. This is clear for pair 4 (with grind G1) and 8 (with grind G3) with almost identical A_{tot}, where pair 4 has twice as long L_a (pair 8 actually has the smallest $L_a = 135$ mm among all the ski pairs). However, the estimated COFs for all three tests are significantly different, most likely because of the significant difference in L_a.

According to Weber et al. [33], the abrasive friction force, F_{abr}, increases with the projected contact area, A_p, and the hardness of the ice or snow surface, H, i.e.,

$$F_{abr} = \tau_{abr} A_p = H A_p \tag{5}$$

For a constant load on the ski, a decrease in the real contact area would result in higher compaction of the snow or ice surface. This effect would also occur if the load increased while the real contact area remained constant. If we represent "load" by the mean apparent pressure, $\overline{P}$, it is reasonable to assert that A_p would increase with increasing $\overline{P}$ and decrease with increasing real contact area, A_r, even though the exact relationship between A_p, $\overline{P}$, and A_r is not explicitly known. Moreover, since the mean apparent pressure increases as the apparent contact length (L_a) decreases, A_p would increase with decreasing L_a. At colder temperatures ($T_s = -13$ °C or lower), the hardness of the snow is presumably higher. However, since an increase in L_a would decrease A_p, the abrasive component of friction is likely to remain largely unchanged.

A key model for adhesive friction (e.g., Glenne [3]) describes the frictional force as the product of the shear strength of the top layer of the softer surface, τ_{adh}, and the real contact area, A_r, i.e.,

$$F_{adh} = \tau_{adh} A_r \tag{6}$$

However, Fig. 5(b) shows that variations in the total real area of contact (A_{tot}) and therefore A_r have minimal impact on the COF. On the other hand, for the colder temperatures ($T_s = -13$ °C or lower), the data indicate that the COF decreases slightly with increasing apparent contact length (L_a). This correlation implies that factors related to L_a are more significant in determining the frictional behaviour. Given that abrasive friction, described by Eq. (5), is influenced by surface interactions and deformation, the observed trend suggests that abrasive friction is the dominant component. The influence of L_a on the COF further supports this conclusion, as changes in L_a would more directly affect abrasive interactions than adhesive ones.

On the occasions with snow temperatures of –3 and –8.5 °C, a shorter apparent contact length resulted in a decrease in the COF. This behaviour cannot be fully explained by the expressions for the adhesive and abrasive friction components in Eqs. (5) and (6). This observation leads to the conclusion that the dominating frictional component might not be adhesive or abrasive friction.

To explore this further, we consider whether the viscous friction could be the dominant frictional component, particularly at a snow temperature of –8.5 °C. To this end, we adopt a model grounded in the linear constitutive relationship of a Newtonian fluid, presented by Makkonen et al. [4–6], expressed as

$$F_{\mathrm{vis}} = \tau_{\mathrm{vis}} A_{\mathrm{w}} = \frac{\eta V A_{\mathrm{w}}}{h} \tag{7}$$

where η is the (constant) fluid viscosity and V the relative velocity of the two surfaces. Here h is typically associated with micro-scale separation; however, if sufficient water is present, macro-scale separation can also contribute to the viscous shear. The wetted area A_{w} is challenging to determine precisely, but Makkonen and Tikanmäki [6] proposed approximating it with the real contact area, i.e., $A_{\mathrm{w}} \approx A_{\mathrm{r}}$.

In this context, both $\min(\bar{h})$ and $\overline{A_{\mathrm{w}}/h}$ are parameters that are presumably linked to viscous friction. However, the data in Fig. 5 do not reveal clear trends, possibly because $\min(\bar{h})$ and $\overline{A_{\mathrm{w}}/h}$ are more relevant under fully flooded conditions.

The apparent contact length (L_{a}), which reflects the area of the ski in contact with the snow, can provide valuable insights, particularly in starved conditions—where liquid water is scarce. In such conditions, direct measurement of the wetted area (A_{w}) becomes challenging. However, given that the current measurements were conducted under conditions where the amount of liquid water was minimal, it is plausible that L_{a} could be used as a proxy to predict A_{w}. As L_{a} increases, it suggests a larger potential area of contact with the snow, which could correspond to a greater wetted area even in minimal water conditions. This concept of using a macroscopic measure like L_{a} to estimate the wetted area aligns with the approach suggested by Ref. [6], where $A_{\mathrm{w}} \approx A_{\mathrm{r}}$, but here it is applied on a larger scale.

4.2 Implications of COF prediction formula

This subsection discusses the linear two-parameter ski–snow friction model (4), designed to quantify the influence of the apparent contact length (L_{a}) and the total real area of contact (A_{tot}) on the COF. The implications of the model results are interpreted in terms of dominant frictional mechanisms, comparing our findings with existing theories and literature to provide a comprehensive understanding of the frictional behaviour of skis on snow.

The selection of apparent contact length (L_{a}) as a predictor in the regression model is justified by the strong correlation between L_{a} and COF across all temperature conditions, as illustrated in Fig. 5. This correlation indicates that L_{a} plays a significant role in influencing the ski–snow friction. While multi-scale parameters such as total real contact area (A_{tot}), minimum average interfacial separation ($\min(\bar{h})$), and integrated average reciprocal interfacial separation ($\overline{A_{\mathrm{w}}/h}$) were considered, they exhibited weaker correlations with the COF. Ultimately, A_{tot} was chosen as the second predictor due to its significant contribution to improving the model's goodness of fit (Fig. 6). The exclusion of $\min(\bar{h})$ and $\overline{A_{\mathrm{w}}/h}$ can be attributed to their lower impact on the model's predictive capability under the tested conditions, likely because these parameters are more relevant under fully flooded or mixed snow conditions, which were not predominant in this study.

The choice of a linear regression model, despite the complex nature of ski–snow friction, was driven by the need for simplicity and interpretability. While non-linear models could potentially capture more intricate relationships between the variables, the linear model with three degrees of freedom offers a balance between model complexity and predictive power. The linear approach was validated by its ability to produce consistent and interpretable results across different snow temperatures, suggesting that the interactions between L_{a}, A_{tot}, and the COF are dominant in the conditions tested. Further exploration of non-linear models could be an avenue for future research, particularly in more variable or extreme snow conditions.

The coefficients in Table 6 indicate that the model behaves differently across the three temperature conditions, reflecting underlying physical changes in the snow influencing the frictional behaviour of the ski–snow contact. The increase in the constant C_0 with decreasing temperature suggests a baseline increase in friction as the snow becomes harder and less lubricated. The positive values of C_1 and C_2 at $T_{\mathrm{s}} = -3$ °C and $T_{\mathrm{s}} = -8.5$ °C indicate that both apparent contact length and total real contact area contribute to an increase in COF under these conditions. In contrast, the negative values of C_1 and C_2 at $T_{\mathrm{s}} = -13$ °C imply that, in much colder conditions, longer L_{a} and larger A_{tot} actually reduce friction, possibly due to a more uniform distribution of load across a harder snow surface, which diminishes the abrasive component of friction. These trends underscore the shifting balance between adhesive and abrasive friction mechanisms as the snow temperature decreases.

The observed correlation between the COF and apparent contact length (L_{a}), as well as total real contact area (A_{tot}), aligns with previous studies. Particularly under different temperature and snow conditions, such as those by Lever et al. [8], which also emphasise the role of contact area in determining friction. However, unlike models that primarily consider micro-scale roughness parameters as dominant predictors [33], our results suggest that macro-scale properties like L_{a} are equally, if not more, critical in colder conditions. This divergence highlights the importance of considering both scales in friction models, particularly when applying them to real-world skiing scenarios where environmental conditions can vary significantly.

Figure 7 shows that there are different optimum combinations of the macro- and multi-scale contact mechanical parameters (L_{a} and A_{tot}) at different snow conditions. The results indicate that when the snow temperature is above −10 °C, the optimal ski-camber profile develops a shorter apparent contact length. However, a ski-camber profile with a longer apparent contact length will exhibit less frictional resistance if the snow temperature is below −10 °C. The results also suggest that a ski-base texture that develops a small total real contact area exhibits less friction when the snow temperature is around −3 °C. The ski-base texture seems to have less influence on the frictional resistance at a snow temperature around −8.5 °C than other snow conditions. In the coldest tested condition, at a snow temperature of −13 °C, the result suggests that a ski-base texture that develops a large total real contact area exhibits the least friction.

As discussed previously regarding the dominating frictional component, based on the constants in Table 6, it is only at warmer temperatures when a decreasing total real contact area decreases the coefficient of friction. This further implies that Eq. (6) does not align with the results obtained herein, whereas Eq. (5), including that A_{p} increases with the mean contact pressure and decreases with real contact area, does align with the results, leading to the conclusion that abrasive friction dominates at colder temperatures.

Previous work by Kalliorinne et al. [19] showed that the total real contact area (A_{tot}) and average reciprocal interfacial separation ($\overline{A_{\mathrm{w}}/h}$) influence each other. Hence, the trend of decreasing friction with decreasing A_{tot} in warmer conditions should not be directly interpreted as indicative of adhesive friction. Furthermore, as mentioned in connection with Eq. (7), the real contact area (A_{r}) has been used as the wetted area (A_{w}), i.e., $A_{\mathrm{r}} = A_{\mathrm{w}}$, in a study by Makkonen and Tikanmäki [6].

Regarding the macro-scale ski-camber profile, the consensus in the ski community is that skis with longer contacting zones are preferred in cold conditions. The results in the present work are consistent with this statement, and in the present work, "colder" is to be associated with hard tracks and snow temperatures around −13 °C or colder. However, approximating the apparent contact area using a feeler gauge height from a ski-camber profile can result in a significant error, as shown in Appendix, where all ski-camber profiles are illustrated with the feeler gauge measurement included.

As for micro-scale ski-base textures, the general consensus is that in colder conditions, a finer, in terms of smaller S_a-value, ski-base texture is the optimum. In contrast, finer ski-base textures usually can develop a larger total contact area [19, 20]. Even though the present work uses relatively rough surfaces, the resulting difference in the total real contact area between the pairs of skis is still in line with the thought that a ski-base texture that develops a larger contact area exhibits lower friction in colder conditions.

4.3 General discussion

The different ski-camber profiles, reflected in the macro-scale contact simulations of the eight ski pairs considered, are important to the objectives of this study. Table 4 shows that the ski pairs have considerably different apparent contact lengths (L_a). Figure 1 and the figures in Appendix also illustrates the differences. For example, Ski 3A (with grind G3) has a rear contact zone with two moderately sharp pressure peaks, indicating concentrated pressure at two specific points, while Ski 6A (also with grind G3) has a rear contact zone with two more concentrated and one significantly higher pressure peak, indicating more intense and localized pressure points, yet both have similar apparent contact lengths (227 and 235 mm, respectively).

It is important to note the discrepancy between the apparent area calculated using the method by Kalliorinne et al. [15] and the area estimated using a 50 μm feeler gauge. This difference is critical when selecting skis based on apparent contact area, as it could influence the prediction of frictional performance. The macro-scale simulation results and the 50 μm feeler gauge estimates for all skis used in this study are provided in Appendix.

Another important observation, as discussed in Kalliorinne et al. [15], is the complexity of accurately approximating the contact mechanical response. For instance, Ski 8A presents an example that a relatively long section of the rear part of the ski appears close to the counter surface but the load is supported at two significantly shorter contact segments, highlighting the challenges in predicting ski performance based solely on estimations of the apparent contact length.

Although the skis with the same grind were ground after one another on the same stone to make the grinds as uniform as possible, the surface roughness parameters may still differ. For example, the S_a-values of grind G2 on Ski pairs 2 and 5 were calculated to be 4.9 and 5.3 μm, respectively. This is quite a significant difference, especially considering that these are the mean values of 10 measurements. However, examining the mean values of the surface parameters listed in Table 3, including the standard deviations, shows that it is possible to distinguish the different ski-base textures.

The BEM simulations revealed some unexpected micro-scale responses. For instance, based on the S_{pk}-value, it is anticipated that grind G1, which exhibits the largest S_{pk}-value, would produce the smallest real area of contact (A_r); however, Fig. 3 shows that G1 (on Ski 1B) actually has a higher A_r than G2 (on Ski 2B) and G3 (on Ski 3B). Additionally, the average reciprocal interfacial separation ($\overline{1/h}$) was expected to follow the inverse of ($\bar{h}$), but G1 and G2 showed similar contact mechanical responses. This pattern was consistently observed across other skis with different grinds. The only parameter aligning with the expectations was $\bar{h}$, with G1 exhibiting the highest value (consistent with the large cavities formed when the narrow peaks separate the surfaces), and in decreasing order for G2 and G3.

Regarding frictional mechanisms, the classical model of adhesive friction disagreed with the current findings from the tests conducted when the snow temperature was −13 °C. Instead, the abrasive friction might be the governing frictional mechanism at this temperature since the results aligned with the governing equation for abrasive friction. From the tests conducted when the snow temperature was −3 and −8.5 °C, both the adhesive and abrasive friction models disagreed with the results in terms of the apparent contact length (L_a). Still, the adhesive friction model agreed with the total real contact area (A_{tot}). However, since L_a was the most significant parameter, this led to the conclusion that viscous friction might be dominating at these conditions and that both L_a and A_r could be used to estimate the wetted area (A_w) but at different scales.

While this study provides significant insights into ski–snow friction, the results are based on specific cold conditions, and further research is needed to generalize these findings across a broader range of environmental factors.

5 Conclusions and future outlook

This study utilized an RTK-GNSS-equipped sled to conduct ski–snow friction tests on eight pairs of cross-country skis with all of the same brand and model but varying ski-camber profiles and ski-base textures. The skis' apparent contact length (L_a) and total real contact area (A_{tot}), calculated using macro- and micro-scale BEM-based models, ranged from 130 to 280 and 23² to 27 mm², respectively. These tests were conducted under three distinct environmental conditions, each representing different snow temperatures.

The findings demonstrate that the apparent contact length—a macro-scale ski property, significantly influences the ski–snow coefficient of friction (COF). Although the correlation between multi-scale contact mechanical properties was less distinct, a simple linear regression model revealed that the total real contact area also played a significant role in determining the COF at the warmest and coldest test conditions, with its influence being larger at $T_s = -13\,^\circ\mathrm{C}$ than $T_s = -3\,^\circ\mathrm{C}$, and almost negligible at the $T_s = -8.5\,^\circ\mathrm{C}$.

The proposed model, with three degrees of freedom, provides a robust framework for quantifying the combined effects of the apparent contact length and total real contact area on the COF. Based on the model, the following guidelines are recommended for minimizing friction in cold conditions on hard tracks:

(1) For snow temperatures above −10 °C, a shorter apparent contact length is preferable. Conversely, a longer apparent contact length is recommended for snow temperatures below −10 °C.

(2) At snow temperatures around −3 °C, minimizing the total real contact area is advantageous.

(3) The total real contact area showed a diminished effect at an intermediate snow temperature of −8.5 °C compared to conditions at −3 and −13 °C.

(4) At the coldest tested condition, with a snow temperature of −13 °C, a ski-base texture developing a larger total real contact area is preferred, as it results in lower friction.

While the current model offers a robust framework for quantifying the effects of the apparent contact length and total real contact area on the COF, future studies could benefit from exploring additional variables such as snow grain size, humidity, and ski base material properties under a wider range of snow conditions. Additionally, incorporating non-linear or interaction terms in the regression model could provide a deeper understanding of the interplay between these factors, particularly in scenarios where multiple friction mechanisms may be simultaneously active. Such advancements could lead to more precise predictions and better guidance for ski selection and preparation.

Appendix

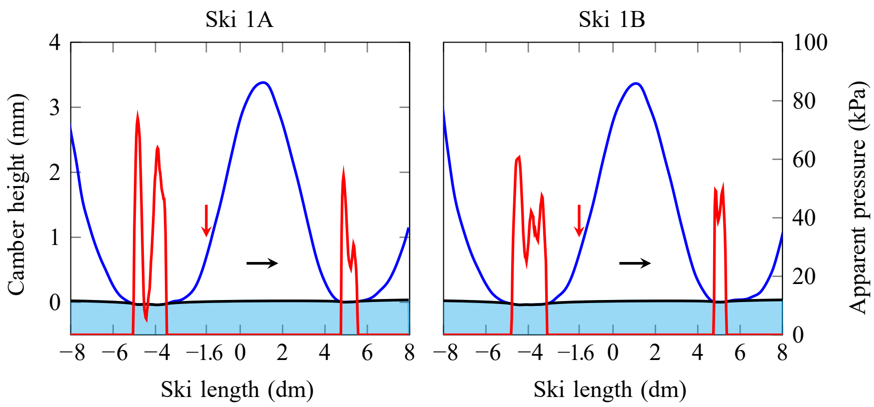

Fig. 8 Macro-scale contact response of two skis corresponding to ski pair 1. Both skis are under an equivalent load of 40 kg, located 1.6 dm behind the balance point and the snow-counter surface is modelled using an elastic modulus of $E_{snow} = 200$ MPa. Ski 1A has an apparent contact length of 158 mm at the rear and 78 mm at the front contact zone, and the corresponding 50 μm feeler gauge measurements of the contact zones are 210 and 157 mm. Ski 1B has an apparent contact length of 168 mm at the rear and 60 mm at the front contact zone, and the corresponding 50 μm feeler gauge measurements of the contact zones are 225 and 180 mm.

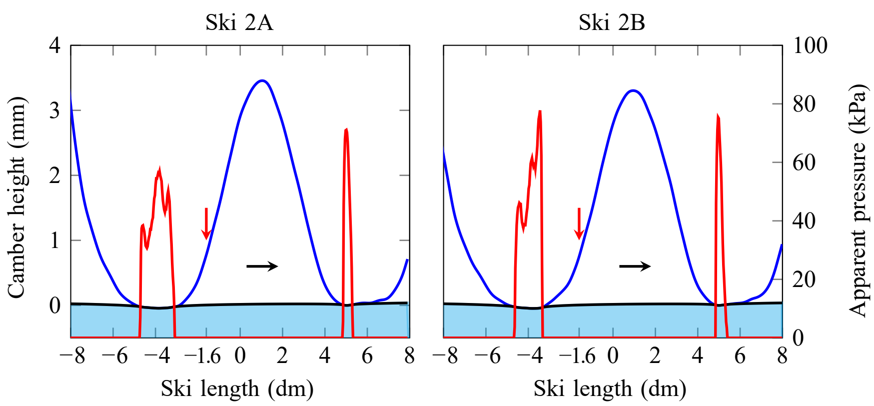

Fig. 9 Macro-scale contact response of two skis corresponding to ski pair 2. Both skis are under an equivalent load of 40 kg, located 1.6 dm behind the balance point, and the snow-counter surface is modelled using an elastic modulus of $E_{snow} = 200$ MPa. Ski 2A has an apparent contact length of 163 mm at the rear and 47 mm at the front contact zone, and the corresponding 50 μm feeler gauge measurements of the contact zones are 207 and 169 mm. Ski 2B has an apparent contact length of 132 mm at the rear and 54 mm at the front contact zone, and the corresponding 50 μm feeler gauge measurements of the contact zones are 170 and 164 mm.

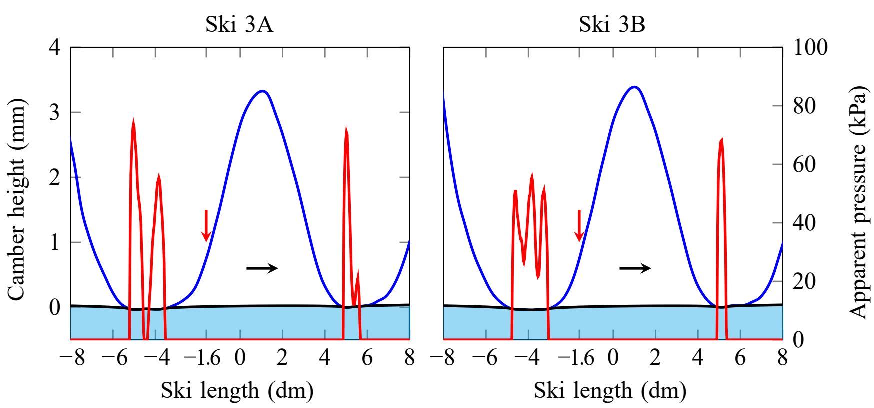

Fig. 10 Macro-scale contact response of the two skis corresponding to ski pair 3. Both skis are under an equivalent load of 40 kg, located 1.6 dm behind the balance point and the snow-counter surface is modelled using an elastic modulus of $E_{snow} = 200$ MPa. Ski 3A has an apparent contact length of 148 mm at the rear and 79 mm at the front contact zone, and the corresponding 50 μm feeler gauge measurements of the contact zones are 224 and 164 mm. Ski 3B has an apparent contact length of 171 mm at the rear and 44 mm at the front contact zone, and the corresponding 50 μm feeler gauge measurements of the contact zones are 218 and 171 mm.

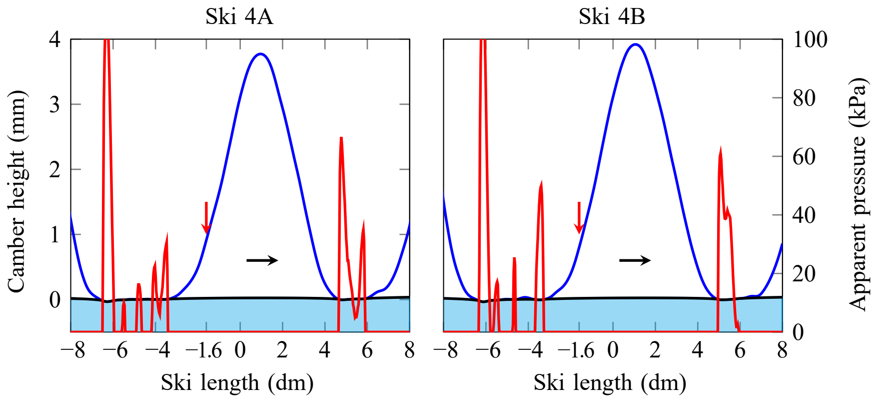

Fig. 11 Macro-scale contact response of the two skis corresponding to ski pair 4. Both skis are under an equivalent load of 40 kg, located 1.6 dm behind the balance point and the snow-counter surface is modelled using an elastic modulus of $E_{\text{snow}} = 200$ MPa. Ski 4A has an apparent contact length of 163 mm at the rear and 124 mm at the front contact zone, and the corresponding 50 μm feeler gauge measurements of the contact zones are 345 and 169 mm. Ski 4B has an apparent contact length of 136 mm at the rear and 97 mm at the front contact zone, and the corresponding 50 μm feeler gauge measurements of the contact zones are 344 and 204 mm.

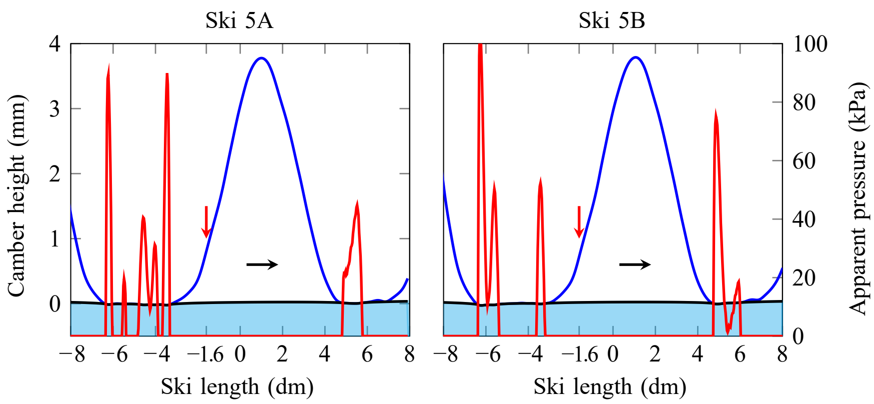

Fig. 12 Macro-scale contact response of the two skis corresponding to ski pair 5. Both skis are under an equivalent load of 40 kg, located 1.6 dm behind the balance point and the snow-counter surface is modelled using an elastic modulus of $E_{\text{snow}} = 200$ MPa. Ski 5A has an apparent contact length of 174 mm at the rear and 94 mm at the front contact zone, and the corresponding 50 μm feeler gauge measurements of the contact zones are 336 and 245 mm. Ski 5B has an apparent contact length of 136 mm at the rear and 127 mm at the front contact zone, and the corresponding 50 μm feeler gauge measurements of the contact zones are 361 and 182 mm.

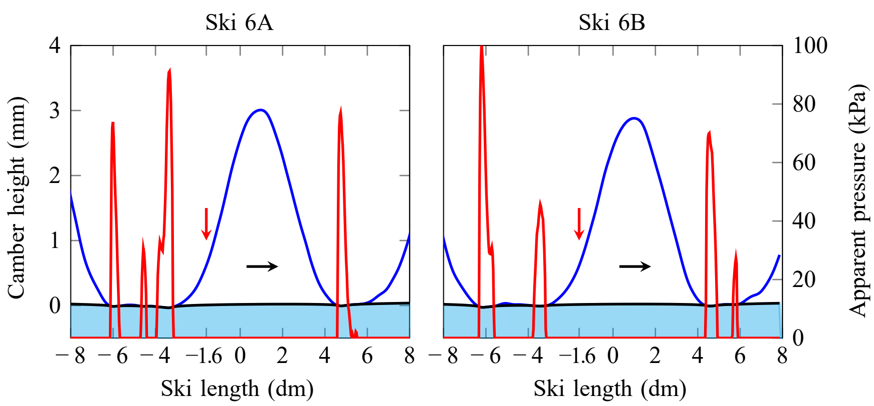

Fig. 13 Macro-scale contact response of the two skis corresponding to ski pair 6. Both skis are under an equivalent load of 40 kg, located 1.6 dm behind the balance point and the snow-counter surface is modelled using an elastic modulus of $E_{\text{snow}} = 200$ MPa. Ski 6A has an apparent contact length of 150 mm at the rear and 85 mm at the front contact zone, and the corresponding 50 μm feeler gauge measurements of the contact zones are 326 and 166 mm. Ski 6B has an apparent contact length of 132 mm at the rear and 84 mm at the front contact zone, and the corresponding 50 μm feeler gauge measurements of the contact zones are 357 and 193 mm.

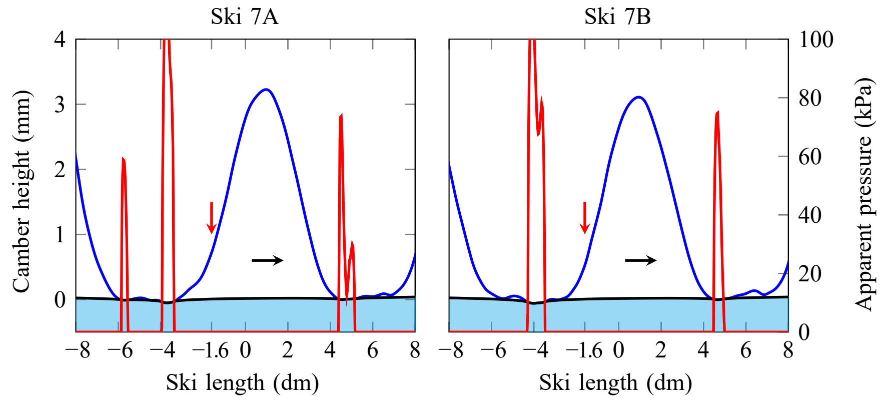

Fig. 14 Macro-scale contact response of the two skis corresponding to ski pair 7. Both skis are under an equivalent load of 40 kg, located 1.6 dm behind the balance point and the snow-counter surface is modelled using an elastic modulus of $E_{snow} = 200$ MPa. Ski 7A has an apparent contact length of 88 mm at the rear and 75 mm at the front contact zone, and the corresponding 50 μm feeler gauge measurements of the contact zones are 130 mm and 195 mm. Ski 7B has an apparent contact length of 82 mm at the rear and 49 mm at the front contact zone, and the corresponding 50 μm feeler gauge measurements of the contact zones are 163 and 127 mm.

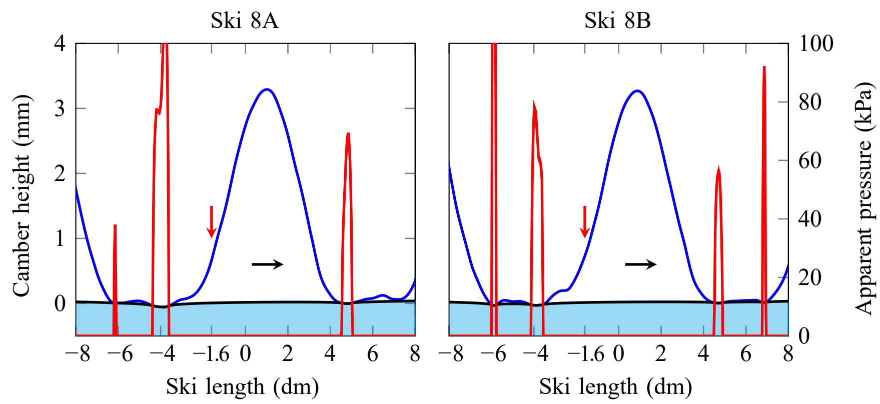

Fig. 15 Macro-scale contact response of the two skis corresponding to ski pair 8. Both skis are under an equivalent load of 40 kg, located 1.6 dm behind the balance point and the snow-counter surface is modelled using an elastic modulus of $E_{snow} = 200$ MPa. Ski 8A has an apparent contact length of 88 mm at the rear and 52 mm at the front contact zone, and the corresponding 50 μm feeler gauge measurements of the contact zones are 114 and 300 mm. Ski 8B has an apparent contact length of 75 mm at the rear and 55 mm at the front contact zone, and the corresponding 50 μm feeler gauge measurements of the contact zones are 267 and 290 mm.

Acknowledgements

The authors would like to acknowledge the assistance from Rikard Larsson and Martin Johansson during testing.

Funding

This research was supported by the Swedish Olympic Committee (SOK) and the Kempe Foundation #JCK-2107.

Declaration of competing interest

The authors have no competing interests to declare that are relevant to the content of this article. The author Roland Larsson is the Editorial Board Member of this journal.

Ethics approval

Not applicable.

Consent to participate

Not applicable.

Consent for publication

All authors consent to the publication of this manuscript.

Availability of data and material

The datasets generated and analysed during the current study are available from the corresponding author upon reasonable request.

Code availability

The code used during the current study is available from the corresponding author upon reasonable request.

Author contributions

Kalle Kalliorinne: conceptualisation, methodology, software, writing - original draft, review & editing; Joakim Sandberg: formal analysis, writing-review & editing; Gustav Hindér: data collection, writing-review & editing; Hans-Christer Holmberg: supervision, writing-review & editing; Matej Supej: writing-review & editing; Roland Larsson: supervision, writing-review & editing; Andreas Almqvist: supervision, project administration, funding acquisition, methodology, writing-review & editing.

References

[1] Almqvist A, Pellegrini B, Lintzén N, Emami N, Holmberg H C, Larsson R. A scientific perspective on reducing ski-snow friction to improve performance in Olympic cross-country skiing, the biathlon and Nordic combined. *Front Sports Act Living* **4**: 844883 (2022)

[2] Street G M, Gregory R W. Relationship between glide speed and Olympic cross-country ski performance. *J Appl Biomech* **10**(4): 393–399 (1994)

[3] Glenne B. Sliding friction and boundary lubrication of snow. *J Tribol* **109**(4): 614–617 (1987)

[4] Makkonen L. Application of a new friction theory to ice and snow. *Ann Glaciol* **19**: 155–157 (1994)

[5] Makkonen L. A thermodynamic model of sliding friction. *AIP ADV* **2**(1): 012179 (2012)
[6] Makkonen L, Tikanmäki M. Modeling the friction of ice. *Cold Reg Sci Technol* **102**: 84–93 (2014)
[7] Lever J H, Taylor S, Song A J, Courville Z R, Lieblappen R, Weale J C. The mechanics of snow friction as revealed by micro-scale interface observations. *J Glaciol* **64**(243): 27–36 (2018)
[8] Lever J H, Taylor S, Hoch G R, Daghlian C. Evidence that abrasion can govern snow kinetic friction. *J Glaciol* **65**(249): 68–84 (2019)
[9] Lever J H, Asenath-Smith E, Taylor S, Lines A P. Assessing the mechanisms thought to govern ice and snow friction and their interplay with substrate brittle behavior. *Front Mech Eng* **7**: 690425 (2021)
[10] Lehtovaara A. *Kinetic Friction between Ski and Snow*. Helsinki (Finland): Finnish Academy of Technology, 1989: 1–52.
[11] Bejan A. The fundamentals of sliding contact melting and friction. *Journal of Heat Transfer* **111**(1): 13–20 (1989)
[12] Bejan A. Contact melting heat transfer and lubrication. *Advances in Heat Transfer* **24**: 1–38 (1994)
[13] Breitschädel F, Berre V, Andersen R, Stjernstrøm E. A comparison between timed and IMU captured Nordic ski glide tests. *Procedia Engineer* **34**: 397–402 (2012)
[14] Kalliorinne K, Hindér G, Sandberg J, Larsson R, Holmberg H C, Almqvist A. The impact of cross-country skiers' tucking position on ski-camber profile, apparent contact area and load partitioning. *P I Mech Eng P—J Spo* 17543371221141748 (2023)
[15] Kalliorinne K, Sandberg J, Hindér G, Larsson R, Holmberg H C, Almqvist A. Characterisation of the contact between crosscountry skis and snow: A macro-scale investigation of the apparent contact. *Lubricants* **10**(11): 279 (2022)
[16] Bäurle L, Kaempfer T U, Szabó D, Spencer N D. Sliding friction of polyethylene on snow and ice: Contact area and modeling. *Cold Reg Sci Technol* **47**(3): 276–289 (2007)
[17] Budde R, Himes A. High-resolution friction measurements of cross-country ski bases on snow. *Phys Eng* **20**(4): 299–311 (2017)
[18] Scherge M, Stoll M, Moseler M. On the influence of microtopography on the sliding performance of cross country skis. *Front Mech Eng* **7**: 659995 (2021)
[19] Kalliorinne K, Persson B N J, Sandberg J, Hindér G, Larsson R, Holmberg H C, Almqvist A. Characterisation of the contact between cross-country skis and snow: A micro-scale study considering the ski-base texture. *Lubricants* **11**(5): 225 (2023)
[20] Kalliorinne K, Hindér G, Sandberg J, Larsson R, Holmberg H C, Almqvist A. Characterisation of the contact between cross-country skis and snow: On the multi-scale interaction between ski geometry and ski-base texture. *Lubricants* **11**(10): 427 (2023)
[21] Schindelwig K, Hasler M, Van Putten J, Rohm S, Nachbauer W. Temperature below a gliding cross country ski. *Procedia Engineer* **72**: 380–385 (2014)
[22] Rohm S, Hasler M, Knoflach C, van Putten J, Unterberger S H, Schindelwig K, Lackner R, Nachbauer W. Friction between steel and snow in dependence of the steel roughness. *Tribol Lett* **59**(1): 27 (2015)
[23] Hasler M, Schindelwig K, Mayr B, Knoflach C, Rohm S, van Putten J, Nachbauer W. A novel ski–snow tribometer and its precision. *Tribol Lett* **63**(3): 33 (2016)
[24] Rohm S, Knoflach C, Nachbauer W, Hasler M, Kaserer L, van Putten J, Unterberger S H, Lackner R. Effect of different bearing ratios on the friction between ultrahigh molecular weight polyethylene ski bases and snow. *ACS Appl Mater Inter* **8**(19): 12552–12557 (2016)
[25] Lemmettylä T, Heikkinen T, Ohtonen O, Lindinger S, Linnamo V. The development and precision of a custom-made skitester. *Front Mech Eng* **7**: 661947 (2021)
[26] Auganæs S B, Buene A F, Klein-Paste A. Laboratory testing of cross-country skis—Investigating tribometer precision on laboratory-grown dendritic snow. *Tribol Int* **168**: 107451 (2022)
[27] Tjørstad R N. An investigation of ski-snow friction. M.D. Thesis. Oslo (Norway): University of Oslo, 2018.
[28] Okajima J, Okabe T, Miyamoto N, Morimoto T, Tsunoda K, Hatakeyama N. Experimental and numerical evaluation of temperature variation by frictional heating at the interface between snow and ski. *J Biomech Sci Eng* **15**(1): 19-00507 (2020)
[29] Sandberg J, Kalliorinne K, Hindér G, Holmberg H C, Almqvist A, Larsson R. A novel free-gliding ski tribometer for quantification of ski–snow friction with high precision. *Tribol Lett* **71**(4): 111 (2023)
[30] Kalliorinne K, Sandberg J, Hindér G, Holmberg H C, Supej M, Larsson R, Almqvist A. Quantifying cross-country ski–snow friction using real-time kinematic positioning. *Friction* **13**(4): 9441011 (2025)
[31] Lintzén N, Edeskär T. Uniaxial strength and deformation properties of machine-made snow. *J Cold Reg Eng* **29**(4): 04014020 (2015)
[32] Tiwari A, Wang A L, Müser M H, Persson B N J. Contact mechanics for solids with randomly rough surfaces and plasticity. *Lubricants* **7**(10): 90 (2019)
[33] Weber B, Nagata Y, Ketzetzi S, Tang F J, Smit W J, Bakker H J, Backus E H G, Bonn M, Bonn D. Molecular insight into the slipperiness of ice. *J Phys Chem Lett* **9**(11): 2838–2842 (2018)

Kalle Kalliorinne defended his thesis entitled "On the multi-scale nature of ski-snow friction: Field testing, characterization and modelling of cross-country ski performance" in April 2024 and is now conducting postdoctoral research at the leading metals research institute Swerim. He is visiting researcher at the Division Machine Elements at Luleå University of Technology and participates in a joint project between Luleå University of Technology, the Swedish Olympic Committee, and the National Teams in Cross-Country Skiing and the Biathlon.

Andreas Almqvist leads the research in computational tribology at the Division of Machine Elements at Luleå University of Technology (LTU). He currently serves as the Editor-in-Chief for the *Proceedings of the IMechE, Part J: Journal of Engineering Tribology*. His scholarly contributions have earned him both best paper awards and other academic honours, and he is also recognized as a Swedish Olympic Committee (SOC) Research Fellow, undertaking sports-tech research. He is the director of the Centre for Sports and Performance Technology at LTU and, in collaboration with SOC and the national teams in Cross-Country Skiing and the Biathlon, he coordinates a variety of activities within the Ski & Snow Laboratory at LTU. More about him and his research endeavours is found on his homepage: https://bit.ly/almqvist